Acta Chemica Scandinavica, 1998: 52: 578–592
Printed in UK all rights reserved

ACTA
CHEMICA SCANDINAVICA
ISSN 0904-213X

Infrared and Raman Spectra and Conformational Equilibrium of Chloromethyl Dimethyl Chlorosilane

Heidi M. Jensen,[a] Peter Klaeboe,[a,*] Valdemaras Aleksa,[a,†] Claus J. Nielsen[a] and Gamil A. Guirgis[b]

[a]Department of Chemistry, University of Oslo, PO Box 1033, 0315 Oslo, Norway and [b]Bayer Corporation, Bushy Park Plant, Research and Development Department, Charleston, SC 29423-8088, USA

Jensen, H. M., Klaeboe, P., Aleksa, V., Nielsen, C. J. and Guirgis, G. A., 1998. Infrared and Raman Spectra and Conformational Equilibrium of Chloromethyl Dimethyl Chlorosilane. – Acta Chem. Scand. 52: 578–592. © Acta Chemica Scandinavica 1998.

The infrared spectra of chloromethyl dimethyl chlorosilane (CH_2Cl–$(CH_3)_2SiCl$) were recorded in the vapour phase and as amorphous and crystalline solids in the 4000–50 cm^{-1} range and isolated in argon, nitrogen and xenon matrices at ca. 5 K. Raman spectra were recorded at room temperature and at various temperatures between 295 and 188 K. Spectra of the amorphous and crystalline solids were obtained at 80 and at 180 K.

The compound exists in two conformations, *anti* and *gauche*, and six infrared and eight Raman bands present in the vapour, liquid and amorphous states vanished after crystallization. The spectra were interpreted in terms of the *anti* conformer being the low energy form in the vapour and liquid phases and also being present in the crystal. The intensity variations with temperature of four band pairs in the Raman spectra of the liquid were employed in van't Hoff plots and gave a value of 0.7 ± 0.2 kJ mol^{-1} for $\Delta_{conf}H$. Very small changes were detected when the matrix spectra were annealed to 35 K (argon) or 32 K (nitrogen). Significant spectral changes were observed when xenon matrices were annealed to 40 K, revealing that the *anti* conformer was also more stable in this matrix.

Ab initio calculations were carried out with the Gaussian 94 program at various levels of approximation including second order Møller–Plesset perturbation; optimized geometries, infrared and Raman intensities and the vibrational frequencies for the *anti* and *gauche* conformers were calculated. After appropriate scaling a reasonably good agreement was obtained between the experimental and calculated wavenumbers for both conformers.

Chloromethyl dimethyl chlorosilane (CH_2Cl–$(CH_3)_2SiCl$), later to be abbreviated CDCS, can *a priori* exist in two conformations, *anti* and *gauche*, as shown in Fig. 1. The compound has been synthesized and investigated by different groups,[1–3] and the infrared and Raman spectra of this compound were first recorded by Hayashi,[4] Batvev *et al.*,[5] Goubeau *et al.*[6] and by Kriegsmann and Engelhardt.[7] All these authors made spectral correlations, but none of them reported the conformational equilibrium in this molecule. A more complete infrared and Raman spectroscopic study was later published by Sera and coworkers,[8] who studied three halogenated silicon compounds, one of which was CDCS. They concluded that two conformers were present for this molecule since six infrared bands of the liquid disappeared in the crystal spectrum.

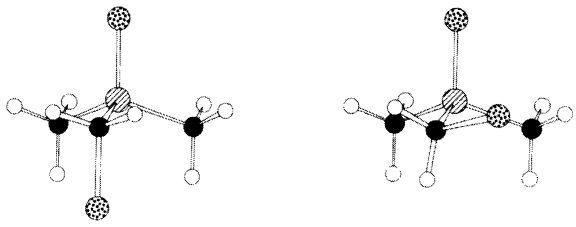

Fig. 1. The *anti* and *gauche* conformers of chloromethyl dimethyl chlorosilane (CDCS).

A number of halogenated silanes with the general structures CH_2Y–$(CH_3)_2SiX$ (Y = Cl, Br; X = H, F, Cl) have lately been synthesized in our laboratories, and we are currently characterizing their conformational properties by infrared and Raman spectroscopy, supported by *ab initio* calculations. Spectra of the vapour and of the amorphous and crystalline samples were recorded in an

* To whom correspondence should be addressed.
† Permanent address: Department of General Physics and Spectroscopy, Vilnius University, Vilnius 2734, Lithuania.

extended infrared region. Moreover, infrared spectra of CDCS isolated in argon, nitrogen and xenon matrices were investigated. Raman spectra of the liquid were obtained at different temperatures and Raman spectra of the crystalline solid were observed. The conformational energies, the structure, the force constants and infrared and Raman intensities were calculated by *ab initio* methods.

It was felt that by investigating a number of related molecules, general trends regarding the Si–C bond relative to the C–C and Si–Si bonds could be evaluated. The effect of various halogen substituents on the conformational stabilities could be studied because of restricted rotation around the Si–C bond. Comparisons can be made with the corresponding spectroscopic studies recently reported for 1,2-dimethyltetrachlorodisilane[9] and 1,1,2,2-tetrachlorodisilane,[10] both of these having a Si–Si bond. Earlier studies included vinyl silanes[11,12] and halogenated silanes: ethyl chlorosilane,[13] ethyldichlorosilane[14] and ethyldifluorosilane,[15] all with conformational equilibria. Preliminary results for CDCS have already been presented; [16] the current paper presents a complete account of the experimental and theoretical results.

Experimental

Sample preparation. The compound was prepared by the reaction of chloro trimethylsilane with sulfuryl chloride, following the procedure of McBride and Beachell.[2] Subsequently, the product was purified in a low temperature, low pressure fractionation column, and the purity was controlled by mass spectrometry.

Spectral measurements. Raman spectra of the liquid, of the amorphous solid and of the crystal were obtained at different temperatures in a capillary tube of 2 mm inner diameter, surrounded by a Dewar, cooled by gaseous nitrogen evaporated from a reservoir.[17] These spectra were employed for estimating the enthalpy difference ΔH between the conformers in the liquid. CDCS and the related halomethyl dimethyl halosilanes all show very pronounced supercooling and it was sometimes possible to study the liquid 50–60 K below the freezing point at 216 K. The crystallization often occurred spontaneously at ca. 160 K when the anisotropic crystal containing only one conformer was obtained. Independently, the vapour of CDCS was condensed on a copper finger at 77 K, and the amorphous and annealed crystalline phases were recorded. The Raman spectra were recorded digitally and obtained using a Dilor RTI-30 spectrometer (triple monochromator) with a Peltier cooled detector. An argon ion laser from Spectra Physics (model 2000) was employed with perpendicular illumination using the 514.5 nm line for excitation.

The infrared spectra were recorded with various Fourier transform spectrometers: a Bruker model IFS-88 (4000–450 cm^{-1}), a Nicolet model 800 (4000–450 cm^{-1}), a Perkin–Elmer model 2000 (4000–450 cm^{-1}) and on two vacuum benches: Bruker IFS-113v spectrometer (600–50 cm^{-1}) and Bomem model DA 3.002 (600–50 cm^{-1}). The latter instrument had a helium cooled Bolometer as detector, the other instruments had detectors of DTGS. Beamsplitters of Ge substrate on KBr were used in the middle infrared regions (MIR) while beamsplitters of Mylar of thickness 3.5, 6 and 12 μm were employed in the far infrared (FIR) region. The vapour was studied in cells with KBr windows and path 10 cm in MIR and in cells of 20 cm and 1 m path with polyethylene windows in the FIR region. The amorphous and crystalline solids were deposited on a CsI and on a wedge shaped window of silicon, cooled with liquid nitrogen, for the MIR and FIR regions, respectively.

The sample was diluted with argon (1:500 and 1:1000), nitrogen and xenon and deposited on a CsI window of a three stage Displex cryostat from APD (model HS-4) at either 5 or 15 K. The matrices were subsequently annealed to various temperatures from 20 K to 35 K (argon), from 20–32 K (nitrogen) and 20–55 K (xenon) in periods from 10 min to 1 h, the window was recooled to 5 K and the spectra recorded.

Results

The infrared and Raman data from all the various states of aggregation are summarized in Table 1.

Infrared spectral results. Vapour spectra of CDCS in the MIR 4000–500 cm^{-1} and FIR regions 600–50 cm^{-1} are given in Figs. 2 and 3, respectively. None of the infrared bands had well resolved rotational contours, and the apparent band structure around 500 cm^{-1} is probably due to a superposition of conformational peaks rather than rotational bands. A FIR spectrum with 0.1 cm^{-1} resolution in the 350–50 cm^{-1} region was recorded with a 1 m path length cell and is presented in Fig. 4. As is apparent, distinct rotational transitions originating from traces of water vapour and from an impurity of HCl are superposed on this spectrum. The bands with centers at 111 and 73 cm^{-1} can be compared with the corresponding infrared transitions at 96 and 67 cm^{-1} in the vapour phase of the related compound bromomethyl dimethyl chlorosilane.[18]

MIR and FIR spectra of the amorphous (solid line) and the annealed crystalline solid (dotted line) at 80 K in the ranges 1450–400 and 650–50 cm^{-1} are shown in Figs. 5 and 6, respectively. Clearly a few infrared bands present in the vapour and in the amorphous phases vanish after crystallization, interpreted as a disappearance of one conformer present in the amorphous solid during crystallization. The vanishing bands are indicated by asterisks in Table 1 and agree with similar observations made in the Raman spectra (see below).

Additional infrared spectra of CDCS were recorded in argon, nitrogen and xenon matrices (1:500 and 1:1000) deposited at 5 and 15 K. Supposedly, the conformational

Table 1. Infrared and Raman spectral data[a] for chloromethyl dimethylchlorosilane (CDCS).

Infrared						Raman			Interpretation	
	Matrix			Solid			Solid		Conformation	
Vapour 289 K	Argon 5 K	Nitrogen 5 K	Xenon 5 K	Amorphous 80 K	Crystal 80 K	Liquid	Amorphous 77 K	Crystal 77 K	*gauche*	*anti*
	2992 m	2989 w			2998 m			3001 s		
2984 m	2987 m	2986 w				2986 m	2990 m	2989 m	ν_1	ν_1
2981 m, 2979 m } B	2982 m				2981 m			2982 s	ν_2	ν_2
2973 m	2977 m	2979 w, 2976 w		2968 s	2968 m	2972 s,P	2974 m	2970 m	$\nu_3\nu_4$	$\nu_3\nu_4$
	2962 m	2962 w, 2960 w, 2956 w	2957 vw							
2952 m, 2948 m, 2945 m } C	2950 w, 2945 w, 2941 w	2950 w, 2945 w, 2941 w		2938 m	2943 s	2938 s,P	2939 m	2944 s	$\nu_5\nu_6$	$\nu_5\nu_6$
	2936 m									
	2920 w	2917 w	2920 vw			2925 m,P		2925 w	ν_7	ν_7
				2906 w	2906 m	2908 vs,P	2906 m	2909 s	ν_8	ν_8
	2858 vw	2854 m	2858 w					2855 w		
						2831 vw		2826 w		
2800 w	2803 w				2795 vw	2795 vw		2802		
	1460 w	1458 w		1463 w	1463 w					
1443 vw	1437 m	1437 w		1438 m	1439 w	1437 vw	1438 w	1439 vw	ν_9	ν_9
	1432 m	1434 m		1437 w	1437 w					
	1424 w	1419 w		1417 m						
	1416 m	1417 m		1415 m	1415 m	1413 m	1411 w	1417 m,br	$\nu_{10}\nu_{11}$	$\nu_{10}\nu_{11}$
1400 m	1404 m	1404 w			1404 m	1400 m,D	1396 m	1398 m	$\nu_{12}\nu_{13}$	$\nu_{12}\nu_{13}$
	1400 m				1401 m					
	1397 m	1398 m			1396 s					
	1392 m									
	1364 w	1363 vw			1364 w					
1269 m										
1266 m	1263 vs, 1261 m, 1259 vs	1264 s			1267 m					
	1258 vs	1258 s		1267 w,br	1262 vs	1260 m,P	1260 m	1260 m	ν_{14}	ν_{14}
1263 vs, 1255 m	1257 vs, 1254 m	1257 s	1257 m,sh↑, 1254 s ↓	1256 s,br	1265 s, 1259 m	1255 m		1254 m	ν_{15}	ν_{15}
1183 m	1184 w, 1181 w	1181 w	1180 w,sh	1185 m	1179 m	1183 m,P	1180 m	*	ν_{16}	
1179 m, 1177 m	1177 m	1178 m	1178 m	1177 s	1176 m, 1174 s	1176 m,P	1177 w,br	1176 m		ν_{16}
1172 m	1172 m	1175 m			1165 m					
	1169 m									
	1113 w↓									
	1105 w↓									
	1102 m	1110 m	1107m↓	1102 m,br	*	1107 m,D	1111 m	*	ν_{17}	
1094 m	1101 w	1103 s	1098 w,sh↑	1096 m,br	1096 m	1098 m,D	1103 m	1099 m		ν_{17}
		1084 m↓	1088 m,sh	1088 w	1088 w	1094 m				
		1082 s	1084 s							
	1080 m,br	1080 s								
	1076 m,br	1076 m↓	1073 s↓						comb.	
	1069 m,br		1065 s							
	1063 m,br									
	1057 m	1070 w		1062 w	1062 w				comb.	
	1055 m									
	1050 m		1051 w,sh							
			1041 w,sh							
	892 vw, 891 w, 888 vw	897 w, 888 w	890 vw, 885 vw	888 w	888 m					
			876 w							
		869 m	867 w↓		865 s	866 w	871 vw	869 m		
		860 vs								
		855 m								
		851 m								

Table 1. (Continued.)

Infrared						Raman			Interpretation	
	Matrix			Solid			Solid		Conformation	
Vapour 289 K	Argon 5 K	Nitrogen 5 K	Xenon 5 K	Amorphous 80 K	Crystal 80 K	Liquid	Amorphous 77 K	Crystal 77 K	*gauche*	*anti*
852 s	857 vs	849 m	854 m↑	855 vs	858 s	853 w	854 m	856 m		ν_{18}
	852 s	841 m	846 s↓						ν_{18}	
	833 s↓	835 m				833 w	834 w	*	ν_{19}	
826 s	828 vs	830 vs		828 vs	828 vs	825 m	829 m	828		ν_{19}
	824 m↓ 819 vs 814 m	819 vs	824 s↑ 822 m,sh 815 s↓	812 vs	~815 s,sh	814 w	815 m	816 m		ν_{20}
803 m										
	811 m 808 m 803 s↓	810 s 802 m	808 m↓ 805 m 802 m↑	805 m,sh	*	805 m	807 m	*	ν_{20}	
	798 s 794 w 787 w	798 m 795 w	798 w,sh 796 w,sh		790 w					
	772 w↓		777 w							
	766 m									
	764 s	766 w								
	763 w		762 w							
	760 s	761 m	750 m↑		762 vs					ν_{21}
760 m	759 w 755 s	756 m 754 m	747 m↓ 742 w,sh	757 vs,br	757 vs	758 s,P	758 s	761 s	ν_{21}	
	733 w			738 m	737 w		735 w	737 w	comb	
		713 vw			730 vw					
705 w	705 m 702 m	705 w 701 m	704 w↓ 701 w	705 m	703 m	705 m	704 m	706 m	ν_{22}	
	697 m	692 m	697 vw↑							ν_{22}
690 mA	695 w	696 w	694 w 690 w↓	692 m	*	693 w	693 m	*	ν_{23}	
	692 w	691 m								
	688 m↓	689 w↓	688 vw							
	687 m 686 m	683 w 678 w	680 w↑	685 m	685 m 681 m	685 m,P	683 m	682 s		ν_{23}
	664 w			663 m	670 m	663 m	664 m	667 m	ν_{24}	ν_{24}
	662 w									
	658 w↓	654 w	653 w↓		654 m	652 vw	652 w	653 m		
	638 w	636 w		637 vw	638 vw 635vw			639 w		
631 s 627 s 623 s	629 s 628 s	633 m 625 s 621 w 618 w	627 m↑ 621 m↑	623 s	624 s 620 s	622 vs,P	624 s	626 vs		ν_{25}
	613 m	615 m↓	615 vw 606 w,sh↑ 603 w↓	611 m	*	614 m,P	612 m	*	ν_{25}	
	576 w	576 w	572 w	~570 vw,br	~575 vw ~565 vw				ν_{26}	ν_{26}
	565 w									
	563 w									
	561 m									
	558 m			551 w	553 m 551 m 549 m					
	546 m									
	540 m									
		526 w		527 w	530 w 522 w	~520 vw				
505 s	499 m	502 w								
500 s	496 s	494 s	493 w↓	483 s		490 m	494 m	*	ν_{27}	
494 s	493 s	490 m	491 w↑		484 vs 477 m	481 vs,P	479 m	482 s		ν_{27}
	491 s									
	488 s	486 m	488 w↓							
	484 w	485 w	483 vw↓							
	481 w									
					465 w					

Table 1. (Continued.)

Infrared						Raman			Interpretation	
	Matrix			Solid			Solid		Conformation	
Vapour 289 K	Argon 5 K	Nitrogen 5 K	Xenon 5 K	Amorphous 80 K	Crystal 80 K	Liquid	Amorphous 77 K	Crystal 77 K	*gauche*	*anti*
298 m				297 s	*	297 m,P	296 m	*	ν_{28}	
263 m				261 s	266 s	264 m,P	265 m	266 m		ν_{28}
				238 m	246 m	238 m	234 m,br	245 m	ν_{29}	ν_{29}
230 m										
				228 m	230 m	229 s,P	229 m,br	234 m	ν_{30}	ν_{30}
					198 m	196 m	196 m	195 m	ν_{31}	ν_{31}
181 m				192 m						
					184 s	190 s,P	189 m	189 m	ν_{32}	ν_{32}
138 w						168 w,P	172 vw,br		$\nu_{33}\nu_{34}$	$\nu_{33}\nu_{34}$
111 m				125 m	128 m	121 m	123 w	125 m	ν_{35}	ν_{35}
								115 m	cryst.	
73 m				100 w	83 w	80 w	~90 m	~85 w,br	ν_{36}	ν_{36}
								77 w	cryst.	
								40 s	cryst.	

[a]Abbreviations: s, strong; m, medium; w, weak; v, very; P, polarized; D, depolorized; A, B and C denote vapour contours; asterisks, bands vanishing in the crystal spectra; arrows pointing upwards or downwards, bands which increase or decrease in intensity after annealing.

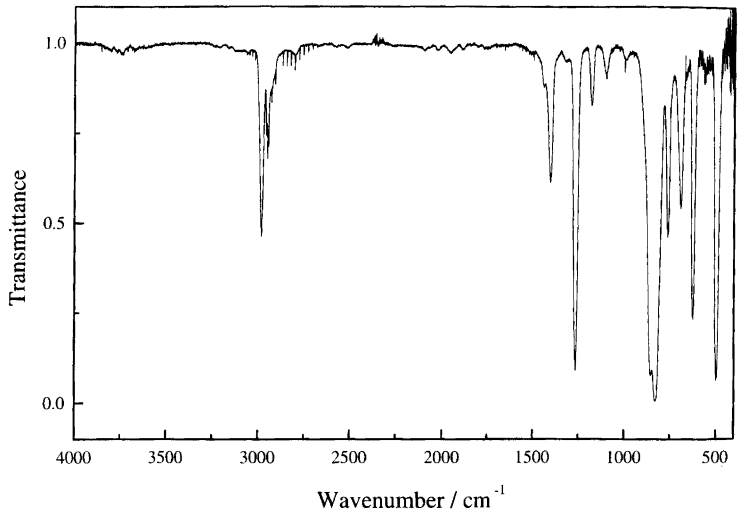

Fig. 2. The infrared vapour spectrum of CDCS in the region 4000–500 cm^{-1} at 17 Torr, path 10 cm.

equilibrium of the vapour phase is maintained when the gas mixture is shock frozen on the CsI window at 5 or 15 K, provided that the barrier to conformational equilibrium is above 3 or 5 kJ mol^{-1}, respectively.[19] Careful annealing of the matrices below 20 K led to small differences due to relaxation of CDCS in the matrix lattice. Quite small spectral changes were also observed in the band intensities of the argon and nitrogen matrices when they were annealed to 35 K for argon and 32 K for nitrogen. Apparently, the conformational equilibrium did not change significantly in this temperature range, suggesting that the conformational barrier is higher than 9 kJ mol^{-1}, preventing the high energy conformer converting to the low energy conformer.[19] Alternatively, the energy difference between the conformers may also be so small that an equilibrium is reached even at these very low temperatures.

For this reason CDCS was also isolated in a xenon matrix in which the vapour pressure of the matrix gas allows annealing to 60 K or higher. It was observed that a number of significant changes occurred when the xenon matrix was heated to 40 K and left at this temperature for ca. 15 min. Annealing to still higher temperatures did not lead to further changes, except that the matrix became 'soft' and the bands appeared broader. Apparently, CDCS diffused in the matrix, forming dimers or larger aggregates. Various detailed matrix spectra are given in Figs. 7–9 showing the infrared spectra recorded before and after annealing. Since the conformational changes appeared at ca. 40 K the barrier can be estimated

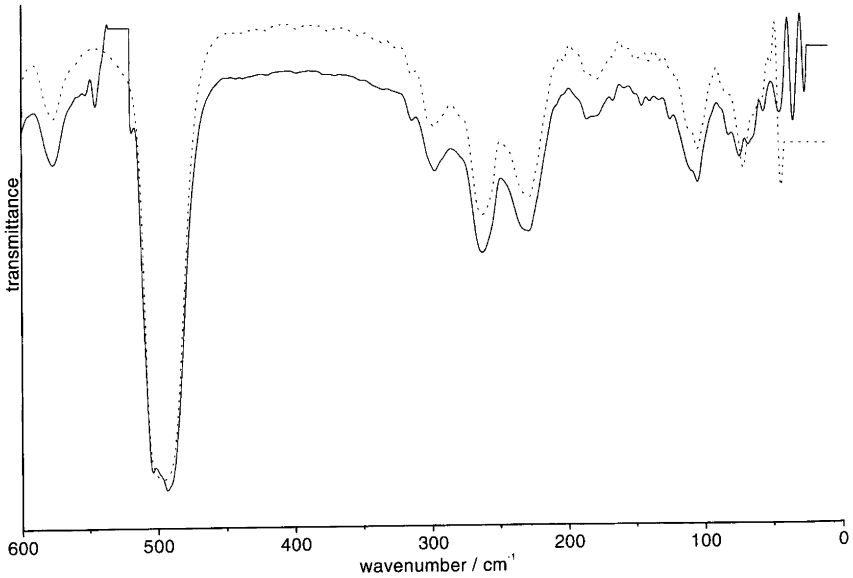

Fig. 3. The far-infrared vapour spectrum of CDCS in the region 600–50 cm^{-1} at 17 Torr, path 20 cm; 3.5 μm beamsplitter, solid line; metal mesh beamsplitter, dashed line.

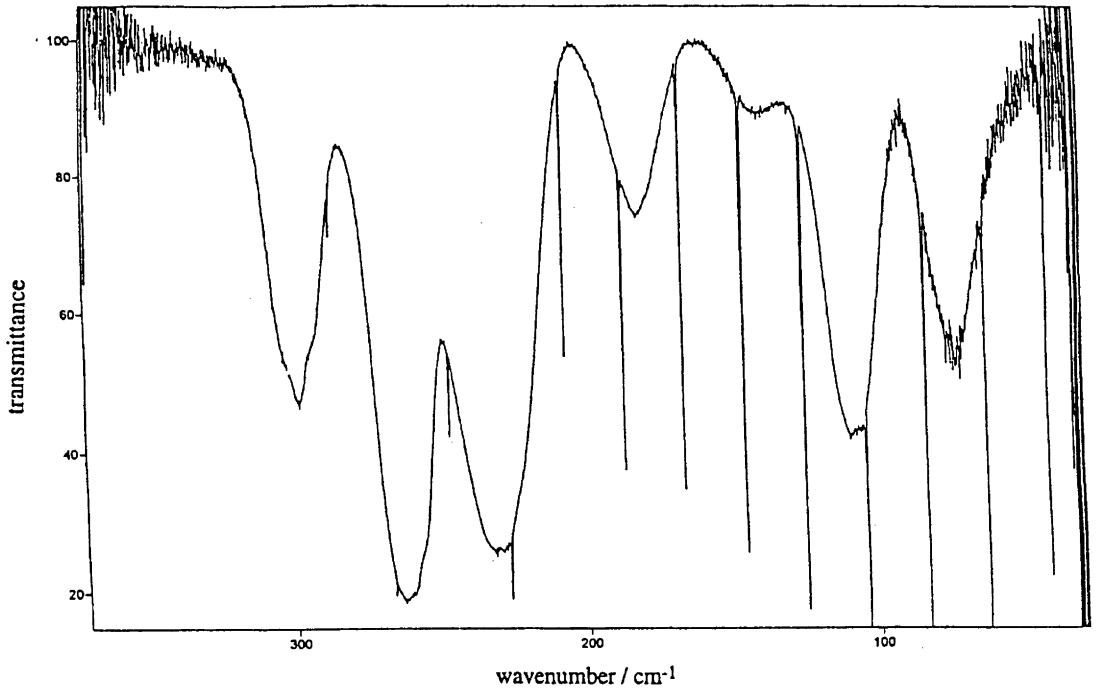

Fig. 4. The infrared vapour spectrum of CDCS in the region 350–50 cm^{-1} at 17 Torr, path 1 m, resolution 0.1 cm^{-1}; an impuritiy of HCl gives rise to sharp rotational bands.

to be 10–12 kJ mol^{-1} from the curves given by Barnes.[19] A much higher barrier of 17.6 kJ mol^{-1} was suggested by Sera *et al.*[8] from a very uncertain estimation of the torsional frequency.

Raman spectral results. Raman spectra of CDCS below 1500 cm^{-1} as a liquid at ambient temperature in two directions of polarization are presented in Fig. 10. A low frequency band, appearing as a shoulder on the Rayleigh line, protrudes clearly at 80 cm^{-1} in the $R(v)$ representation[20] of the Raman spectrum, Fig. 11. Additional Raman spectra were recorded between 295 and 188 K in a Dewar cooled by a stream of cold nitrogen gas[17] (the latter temperature represented a strongly supercooled liquid since the melting point is close to 216 K). A spontaneous crystallization occurred at ca. 160 K and a

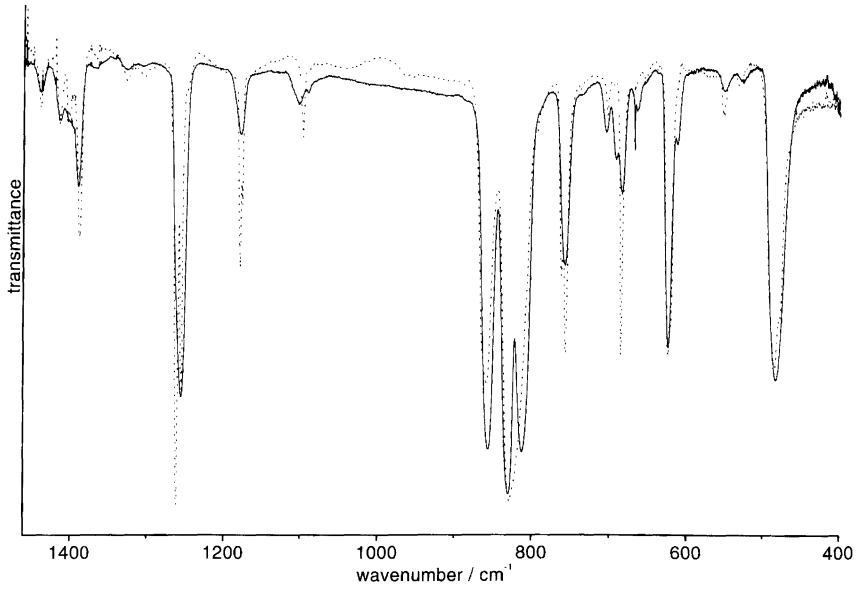

Fig. 5. The infrared spectra (1450–400 cm^{-1}) of amorphous (solid line) and crystalline (dashed line) of CDCS at 80 K.

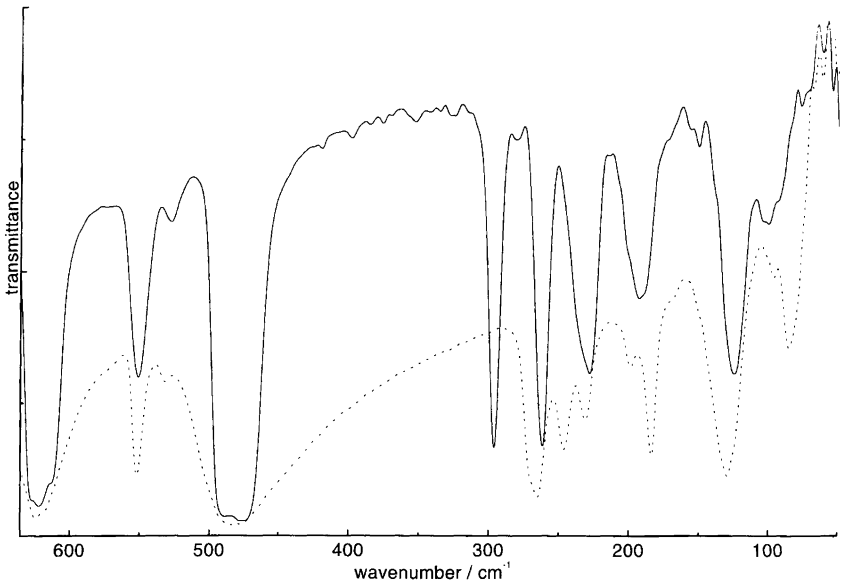

Fig. 6. The far-infrared spectra (600–50 cm^{-1}) of amorphous (solid line) and crystalline (dashed line) of CDCS at 80 K.

Raman spectrum of the crystal was recorded at 200 K. An independent Raman spectrum of an amorphous and an annealed crystal was obtained by depositing the vapour on a cold finger of copper at 80 K, cooled by liquid nitrogen and subsequent annealing; the spectrum was quite similar to that formed by cooling the liquid. Raman spectra of the liquid and of the crystalline solid at 77 K are compared in Fig. 12. As can be seen, some Raman bands present in the liquid vanished in the Raman spectrum of the crystal (indicated with asterisks in Table 1), and they correspond to those vanishing in the infrared spectra (Figs. 5 and 6). They are attributed to the second conformer which disappears in the crystal. However, the number of vanishing bands is small, and most of the fundamentals of one conformer presumably overlap those of the other conformer.

Slight intensity variations of certain bands were observed in the variable temperature Raman spectra of the liquid, and the bands which vanished in the crystal were enhanced at higher temperatures. This effect was interpreted as a displacement of the conformational equilibrium, and a quantitative evaluation of the enthalpy difference was carried out. The following band pairs (cm^{-1}) were selected: 297*/264, 614*/622, 1107*/1098 and 1183*/1176, in which the first band of the pair represents the conformer vanishing in the crystal while

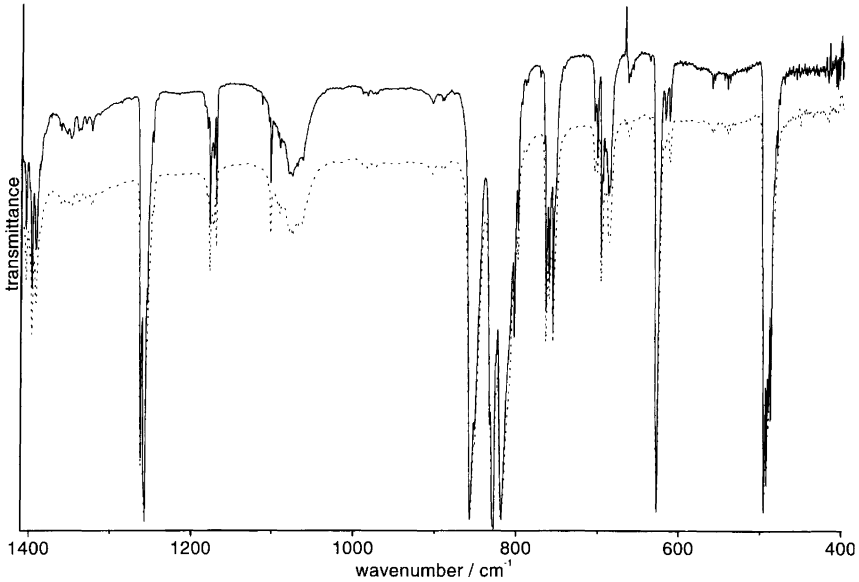

Fig. 7. Infrared spectra of CDCS (1450–400 cm^{-1}) in an unnannealed argon matrix (1:1000) at 5 K (solid line) and annealed to 35 K (dashed line).

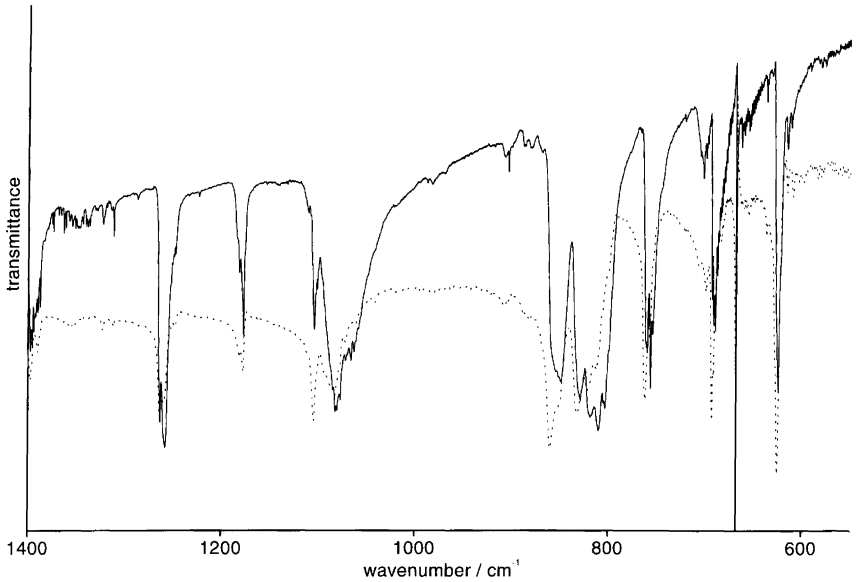

Fig. 8. Infrared spectra of CDCS (1450–600 cm^{-1}) in a nitrogen matrix (1:1000) at 5 K, unannealed (solid line) and annealed to 32 K (dashed line).

the second (generally a neighboring band) is tentatively attributed to the conformer present in the crystal. However, the second band may also have contributions from the high energy conformer, making it unsuited for quantitative calculations.

Assuming $\Delta_{conf}H$ to be constant, the temperature variation of the intensity ratio for each band pair, I^*/I, was fitted to the equation:

$$\ln\left(\frac{I_T^*}{I_T}\right) = -\frac{\Delta_{conf}H}{RT} + \left(\frac{\Delta_{conf}S}{R} + C\right)$$

where C is a constant depending on the molar scattering coefficients for the bands in question of the two conformers. Independent van't Hoff plots were based upon peak heights and integrated band areas of each pair. With the exception of the pair 297*/264 cm^{-1}, the integrated band areas showed a large scatter of the points and appeared less suited for the quantitative calculations. Table 2 summarizes the results of van't Hoff plots based upon measured peak heights and an additional plot based upon the integrated areas of the 297*/264 cm^{-1} band pair; the average value $\Delta_{conf}H = 0.7 \pm 0.2$ kJ mol^{-1} was derived from these data. To be discussed below, the low energy conformer, which is also present in the crystal, is probably *anti*.

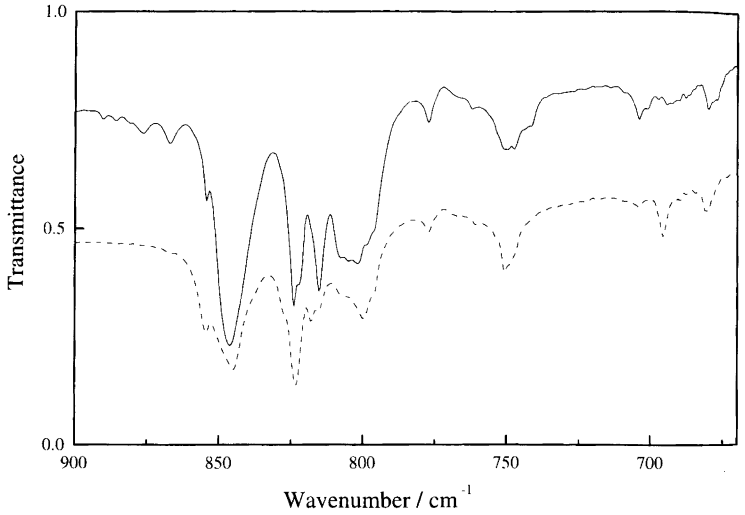

Fig. 9. Infrared spectra of CDCS (900–640 cm^{-1}) in a xenon matrix (1 : 1000) at 5 K, unannealed, solid line; annealed to 40 K, dashed line.

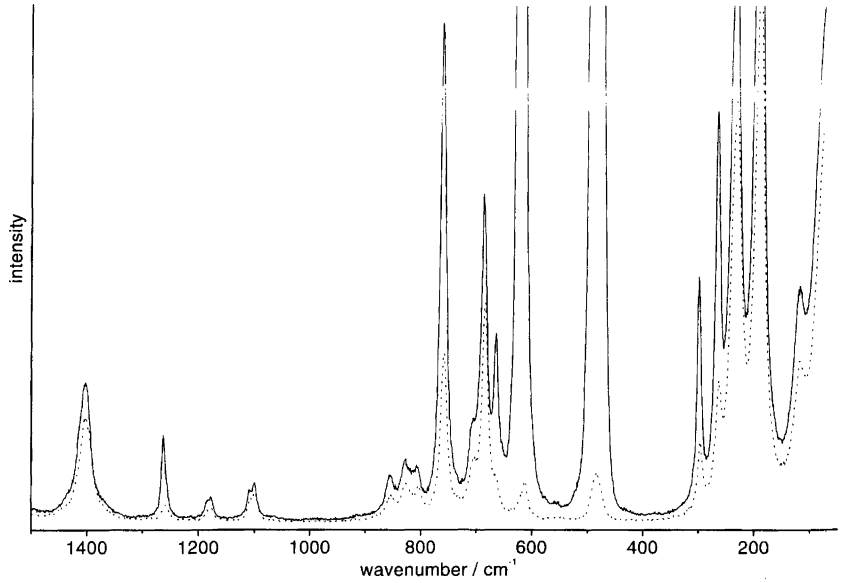

Fig. 10. Raman spectra of CDCS as a liquid below 1500 cm^{-1}, in two polarization directions.

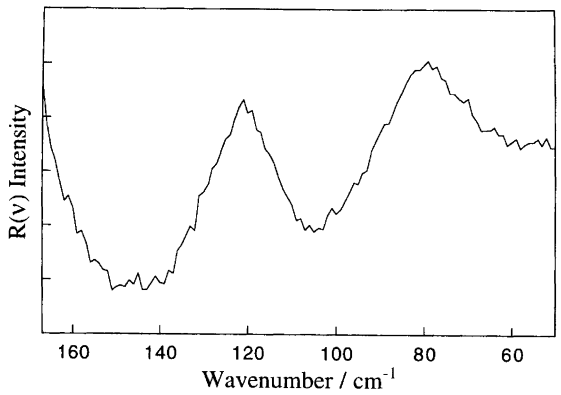

Fig. 11. The Raman spectrum (170–50 cm^{-1}) of CDCS at ambient temperature in the *R*(v) representation.

Quantum chemical calculations. Ab initio calculations of CDCS were carried out using the Gaussian 94 program[21] with a variety of basis functions (see below). Two minima on the potential energy surface, corresponding to *anti* and *gauche*, were found by simultaneously relaxing all geometric parameters according to the conventional Berny procedure. The dihedral angle ∠Cl–Si–C–Cl of the *gauche* conformer was calculated to be 69°, but otherwise only small differences were found in the bond lengths and bond angles between the conformers of CDCS. The Si–C bond was calculated to be 189 pm for both the *anti* and *gauche* conformers compared to 154 pm expected for a C–C single bond. The longer Si–C distance compared to the C–C distance in ethanes should contribute to a weaker interaction between the two parts of the molecule, resulting in a lower enthalpy difference between

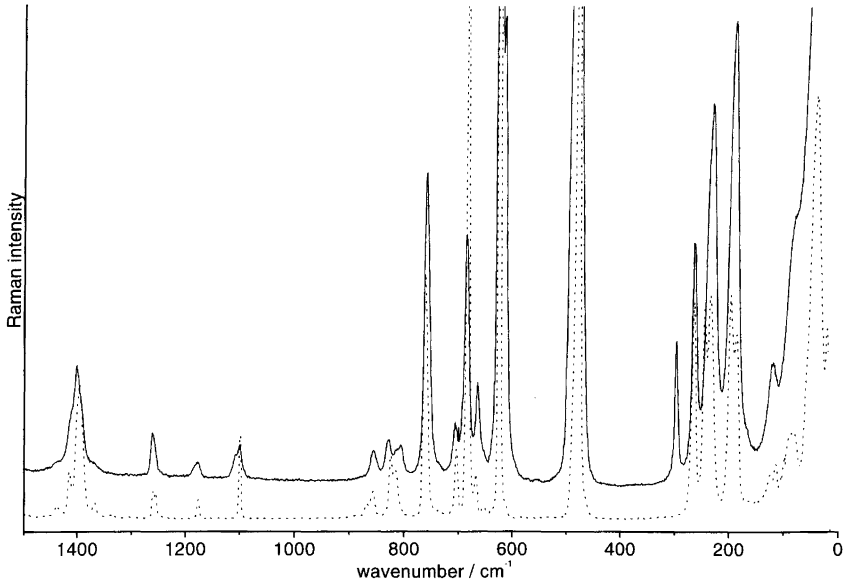

Fig. 12. The Raman spectra of CDCS as a liquid (solid line) and as a crystalline solid (dashed line) at 77 K below 1500 cm^{-1}.

Table 2. Derived $\Delta_{conf}H$ from van't Hoff plots.

Band pair	Method[a]	$\Delta_{conf}H$	σ^b
297*/264	Peak heights	0.60	0.09
297*/264	Integrated band area	0.9	0.4
614*/624	Peak heights	1.06	0.15
1107*/1099	Peak heights	0.48	0.20
1183*/1176	Peak heights	0.73	0.21
Average		0.7	0.2

[a]See text. [b]σ represents 1 standard deviation in the derived $\Delta_{conf}H$.

the conformers and many overlapping conformer bands compared to the corresponding ethane derivative.

The difference conformational energy, derived from the following six levels of approximation HF/3-21G*, HF/6-31G*, HF/6-31G**, HF/6-311G*, MP2/6-31G* and MP2/6-311G* were as follows: 6.0, 6.8, 6.6, 6.6, 6.6, 6.5 and 6.3 kJ mol^{-1}. The dipole moments of the two conformers were calculated as ca. 1 D for the *anti* and ca. 3.7 D for the *gauche*. The calculations all gave *anti* as the low energy conformer. However, the level of accuracy when utilizing these restricted basis sets is comparable to the calculated energy differences. Thus, it is not surprising that these values were nearly an order of magnitude higher than the experimental value of 0.7 kJ mol^{-1} which was obtained from the variable temperature Raman spectra of the liquid. It should also be emphasized that the calculated *ab initio* energies refer to the vapour phase, while a stabilization of the *gauche* conformer energy is expected in the liquid compared to the vapour phase, due to the large dipole moment of the *gauche* compared to the *anti* conformer. In the series of halomethyl dimethyl halosilanes investigated[22] the *anti* conformer was invariably the low energy conformer according to the *ab initio* calculations.

Normal coordinate calculations. A set of analytical force constants were derived for each of the two conformers in the HF/6-311G* calculations. The large bulk of force constants are not reported for the sake of brevity. The calculated *ab initio* force constants were subsequently transformed from Cartesian to a set of symmetry valence coordinates. As generally observed for *ab initio* calculated wavenumbers, those listed as ν_{calc} in Tables 3 and 4 for *anti* and *gauche*, respectively, are invariably larger than the experimental values. In order to make a complete assignment of the observed IR and Raman bands, a normal coordinate analysis with scaled force constants was also carried out.

Various scaling factors to the different types of motions were tested in an iteration procedure. In essence, an equally good agreement between the experimental and calculated wave numbers was achieved by using scaling factors of 0.9 for the stretching and bending modes above, and 1.0 for the modes below 400 cm^{-1}. In addition, Tables 3 and 4 include infrared intensities, Raman scattering cross-sections and the Raman polarization ratios, ρ. The calculated intensities should be considered as very approximate, although they served as a guideline during the spectral assignments.

The PED (potential energy distributions) listed in Tables 3 and 4 are expressed in terms of the symmetry coordinates which are given in Table 5 and they are defined from the internal coordinates described in Fig. 13. Only PED terms larger than 10% have been included in Tables 3 and 4. The C–H, C–Cl and Si–Cl stretching modes are all fairly well localized, but the CH_3 rock, C–C stretches and the skeletal deformations are highly

Table 3. Calculated and observed fundamentals of the *anti* conformer of chloromethyl dimethyl chlorosilane (CDCS).

Vib. no.		ν_{calc}[a]	ν_{calc}[b] scaled	I_{IR}[c] int.	I_R[d] int.	Dep.	ν_{obs}[e]	I_{IR}	I_R	PED[f]
ν_1	*A″*	3311	2980	3.3	66.2	0.75	2986	m	m	S22(100)
ν_2	*A′*	3252	2927	21.3	112.1	0.20	2986[g]	m	m	S5(89), S7(10)
ν_3	*A′*	3249	2924	9.1	81.8	0.68	2972	m	s,P	S7(89), S5(10)
ν_4	*A″*	3249	2924	8.9	50.1	0.75	2972	m	s,P	S24(99)
ν_5	*A′*	3247	2923	23.2	141.3	0.75	2938	m	s,P	S8(99)
ν_6	*A″*	3245	2920	0.0	15.9	0.75	2938	m	s,P	S25(99)
ν_7	*A′*	3177	2860	3.2	224.4	0.00	2925	w	m,P	S6(100)
ν_8	*A″*	3176	2858	5.8	0.2	0.75	2908	w	vs,P	S23(100)
ν_9	*A′*	1598	1438	5.5	0.4	0.69	1437	w	vw	S19(80)
ν_{10}	*A′*	1593	1433	9.7	9.8	0.75	1413	m	m	S18(83), S19(11)
ν_{11}	*A″*	1585	1427	2.7	3.9	0.75	1413	m	m	S33(79), S34(17)
ν_{12}	*A″*	1583	1425	0.3	11.9	0.75	1400	m	m,D	S34(79), S33(17)
ν_{13}	*A′*	1577	1419	16.1	14.1	0.74	1400	m	m,D	S13(88)
ν_{14}	*A′*	1450	1305	19.7	2.9	0.02	1260	vs	m,P	S15(95)
ν_{15}	*A″*	1444	1300	44.6	0.1	0.75	1257	vs	m	S30(95)
ν_{16}	*A′*	1348	1213	8.1	1.2	0.44	1176	s	m,P	S14(92)
ν_{17}	*A″*	1240	1116	1.1	5.0	0.75	1098[h]	m	m,D	S28(95)
ν_{18}	*A′*	957	862	86.5	0.8	0.34	854	s	w	S16(73), S2(10)
ν_{19}	*A′*	924	831	122.9	0.6	0.30	825	vs	m	S17(74)
ν_{20}	*A″*	916	824	93.8	0.0	0.75	815	m	w	S29(36),S31(25), S21(18)
ν_{21}	*A″*	848	763	13.5	1.7	0.75	750[g]	vs	s,P	S32(70), S31(11), S21(10)
ν_{22}	*A′*	815	734	21.4	11.9	0.47	697[g]	m	w	S2(49), S4(35)
ν_{23}	*A″*	760	684	7.6	2.9	0.75	685	m	m,P	S31(47), S21(43)
ν_{24}	*A″*	750	675	0.8	2.9	0.75	663	m	m,P	S29(47), S21(18), S32(14), S28(13)
ν_{25}	*A′*	725	652	26.1	13.4	0.71	622	m	m	S4(41), S2(20), S1(14)
ν_{26}	*A′*	646	582	56.0	16.6	0.01	575	s	vs,P	S1(60), S4(15)
ν_{27}	*A′*	511	460	99.8	9.8	0.08	481	vs	vs,P	S3(70), S9(10)
ν_{28}	*A′*	281	281	9.2	2.2	0.44	264	s	m,P	S9(26), S12(27), S13(13), S17(13)
ν_{29}	*A″*	244	244	6.7	1.9	0.75	238	m	m	S27(44), S26(32), S29(10)
ν_{30}	*A′*	233	233	7.9	1.7	0.66	229	m	s,P	S11(55), S16(20), S9(13)
ν_{31}	*A′*	193	193	0.2	2.1	0.68	196	m	m	S10(36), S12(18), S9(16)
ν_{32}	*A″*	188	188	1.6	0.8	0.75	190	s	s,P	S26(44), S27(37)
ν_{33}	*A′*	168	168	0.0	0.0	0.62	168	w	w,P	S20(98)
ν_{34}	*A″*	158	158	0.1	0.0	0.75	168	w	w,P	S36(98)
ν_{35}	*A′*	118	118	5.8	0.3	0.74	121	m	m	S12(40), S10(20), S13(16), S11(11)
ν_{36}	*A″*	72	72	4.6	0.9	0.75	80	w	w	S35(92)

[a]Calculated at the HF/6-311G* level in Gaussian 92. [b]Scaled with a factor of 0.9 above and 1.0 below 400 cm^{-1}. [c]Infrared intensities in $km^2\ mol^{-1}$. [d]Raman intensities in $Å^4\ mol^{-1}$. [e]From Raman spectra of the liquid, except when noted. [f]Contributions below 10% are omitted. [g]From IR crystal spectra. [h]From Xe matrix spectra.

mixed. As expected, in the *gauche* conformer in which all the vibrational modes belong to the same symmetry species, the modes are more mixed than in the *anti* conformer with two symmetry species *A′* and *A″*.

Discussion

Conformations. The calculated *ab initio* energies (see above) reveal an energy difference of ca. 6.5 kJ mol^{-1} with *anti* being the low energy conformer, but due to the large uncertainties inherent in these calculations the is result is not conclusive. In the series of five molecules with the structure CH_2Y-$(CH_3)_2SiX$ investigated, *anti* was invariably calculated[22] to be the low energy conformer using the basis set HF/6-311G* with values ranging from 7.4 to 1.3 kJ mol^{-1}. Since the contours in the infrared vapour spectra are poorly resolved (cf. Figs. 2–4), they cannot be made a basis for determining the conformers.

If the six hydrogens in the two methyl groups are oriented symmetrically to the symmetry plane, the *anti* conformer has C_s symmetry while the *gauche* conformer has no symmetry (Fig. 1). The 36 fundamentals in the *anti* conformer will divide themselves between 20 of symmetry species *A′* and 16 of species *A″* of which the former will give rise to polarized, the latter to depolarized bands in the Raman spectra. In the *gauche* conformer without symmetry all the 36 fundamentals will obviously

Table 4. Calculated and observed fundamentals of the *gauche* conformer of chloromethyl dimethyl chlorosilane (CDCS).[a]

Vib. no.	ν_{calc}[a]	ν_{calc} scaled	I_{IR} int.	I_R int.	Dep.	ν_{obs}	I_{IR}	I_R	PED
ν_1	3294	2965	5.1	71.6	0.72	2986	m	m	S22(97)
ν_2	3263	2936	8.0	68.6	0.74	2986[b]	m	m	S7(49), S24(46)
ν_3	3248	2923	14.1	92.3	0.75	2972	m	s,P	S24(41), S7(37), S8(13)
ν_4	3237	2914	29.5	143.3	0.74	2972	m	s,P	S8(70), S5(12)
ν_5	3235	2911	10.9	70.3	0.14	2938	m	s,P	S5(59), S25(32)
ν_6	3234	2910	9.8	52.0	0.21	2938	m	s,P	S25(49), S5(25), S8(11)
ν_7	3173	2856	9.3	175.8	0.02	2925	w	m,P	S6(73), S23(22)
ν_8	3170	2853	6.1	59.2	0.01	2908	w	vs,P	S23(74), S6(23)
ν_9	1599	1440	11.5	2.0	0.73	1437	w	vw	S19(84), S18(10)
ν_{10}	1591	1432	4.3	13.1	0.75	1413	m	m	S18(81), S19(10)
ν_{11}	1587	1428	2.5	7.0	0.75	1413	m	m	S34(51), S33(40)
ν_{12}	1583	1425	2.3	12.6	0.75	1400	m	m,D	S33(41), S34(44)
ν_{13}	1575	1418	11.6	8.1	0.71	1400	m	m,D	S13(80), S33(13)
ν_{14}	1450	1305	21.4	3.3	0.01	1260	vs	m,P	S15(95)
ν_{15}	1443	1300	41.5	0.2	0.29	1254[b]	vs	m	S30(94)
ν_{16}	1354	1218	7.6	1.0	0.36	1183	m	m,P	S14(93)
ν_{17}	1250	1125	1.4	5.8	0.75	1107	m	m,D	S28(95)
ν_{18}	954	859	99.8	0.8	0.51	886[b]	s	w	S16(71)
ν_{19}	939	845	146.1	0.5	0.58	833	vs	w	S17(61), S29(10)
ν_{20}	878	790	77.5	0.6	0.74	805	m	m	S31(37),S21(27)
ν_{21}	844	759	9.2	1.3	0.52	747[b]	vs	s,P	S32(81)
ν_{22}	827	745	2.7	17.0	0.45	704[b]	m	w	S4(50), S2(23)
ν_{23}	772	694	30.7	0.9	0.75	693	m	m	S29(49), S28(11)
ν_{24}	754	679	8.8	6.5	0.71	663	m	m,P	S21(57), S31(36)
ν_{25}	703	633	29.9	5.0	0.34	614	m	m	S2(36), S1(26), S4(11), S29(11)
ν_{26}	645	580	35.6	16.2	0.13	575	m	m,P	S1(30), S4(18), S12(16)
ν_{27}	501	451	69.4	10.3	0.07	490	vs	m	S3(80)
ν_{28}	318	286	21.6	3.6	0.53	297	s	m,P	S12(35), S13(17), S27(11)
ν_{29}	239	239	9.8	1.8	0.69	238	m	m	S26(20), S11(24), S10(16), S27(11)
ν_{30}	233	233	2.5	1.4	0.75	229	m	s,P	S9(71), S17(14)
ν_{31}	198	198	0.9	2.1	0.69	196	m	m	S11(37), S26(22)
ν_{32}	185	185	0.8	1.0	0.71	190	s	s,P	S10(23), S26(28), S27(20)
ν_{33}	173	173	0.1	0.0	0.67	168	w	w,P	S20(90)
ν_{34}	161	161	0.0	0.0	0.70	168	w	w,P	S36(97)
ν_{35}	122	122	1.1	0.4	0.71	121	m	m	S12(41), S27(21), S13(19)
ν_{36}	63	63	2.1	1.6	0.75	80	w	w	S35(89)

[a]For abbreviations, see footnote to Table 2. [b]From IR crystal spectra.

give rise to polarized Raman bands, but these criteria are of limited value in the assignments.

As is apparent from Table 1 the Raman bands (liquid) at: 1183, 1107, 833, 805, 693, 614, 490 and 297 cm^{-1} vanished during crystallization. The infrared counterparts also disappeared on crystallization in the corresponding infrared spectra except for the band at 1179 cm^{-1}. However, this band appeared as a shoulder on the infrared bands at 1176 and 1174 cm^{-1}. Moreover, only one infrared band was observed in the spectra of the amorphous and crystalline solids at 828 and 483 cm^{-1}, whereas two separate conformer bands were seen in the Raman spectra of both, in which one disappeared after crystallization (Table 1). The vanishing bands undoubtedly belong to the conformer which is not present in the crystal. It is seen from Table 1 that many of the disappearing bands also loose intensity in the infrared spectra of CDCS in the Xe matrix after annealing. From the Raman spectra recorded at various temperatures they are also enhanced in intensity with temperature. In other instances the *anti* and *gauche* bands overlap in the infrared and Raman spectra, but appear as separate bands in the matrices. From the observed intensity changes among the infrared bands of CDCS in the Xe matrices, the bands around 1255, 855, 757 and 705 cm^{-1} seem to be split into *anti* and *gauche* components after annealing.

The most reliable criterion for assigning the bands to *anti* and/or *gauche* involves correlating the infrared and Raman bands vanishing in the crystal with the scaled *ab initio* wavenumbers for the *anti* (Table 3) and *gauche* (Table 4) fundamentals. Below 1300 cm^{-1} nine instances

Table 5. Symmetry coordinates for chloromethyldimethyl chlorosilane (CDCS).

A'		
1	Si–C symmetric stretch	$S_1 = 3^{-1/2}(R_1 + R_2 + R_3)$
2	Si–C antisymmetric stretch	$S_2 = 6^{-1/2}(2R_1 - R_2 - R_3)$
3	Si–Cl stretch	$S_3 = S$
4	C–Cl stretch	$S_4 = T$
5	CH_2 symmetric stretch	$S_5 = 2^{-1/2}(s_7 + s_8)$
6	CH_3 symmetric stretch	$S_6 = 6^{-1/2}(d_1 + d_2 + d_3 + d_4 + d_5 + d_6)$
7	CH_3 antisymmetric stretch	$S_1 = 12^{-1/2}(2d_1 - d_2 - d_3 + 2d_4 - d_5 - d_6)$
8	CH_3 antisymmetric stretch	$S_8 = \frac{1}{2}(d_2 - d_3 + d_5 - d_6)$
9	Symmetric C–Si–C bend	$S_9 = 6^{-1/2}(\Xi_1 + \Xi_2 + \Xi_3 - \Phi_1 - \Phi_2 - \Phi_3)$
10	Antisymmetric C–Si–C bend	$S_{10} = 6^{-1/2}(2\Xi_1 - \Xi_2 - \Xi_3)$
11	Antisymmetric C–Si–C bend	$S_{11} = 6^{-1/2}(2\Phi_1 - \Phi_2 - \Phi_3)$
12	Si–C–Cl bend	$S_{12} = \Omega$
13	CH_2 scissor	$S_{13} = \frac{1}{2}(\gamma_1 + \gamma_2 + \theta_1 + \theta_2)$
14	CH_2 wag	$S_{14} = \frac{1}{2}(\gamma_1 + \gamma_2 - \theta_1 - \theta_2)$
15	CH_3 symmetric deformation	$S_{15} = 12^{-1/2}(\beta_1 + \beta_2 + \beta_3 - \alpha_1 - \alpha_2 - \alpha_3 + \beta_4 + \beta_5 + \beta_6 - \alpha_4 - \alpha_5 - \alpha_6)$
16	CH_3 antisymmetric deformation	$S_{16} = 12^{-1/2}(2\beta_1 - \beta_2 - \beta_3 + 2\beta_4 - \beta_5 - \beta_6)$
17	CH_3 antisymmetric deformation	$S_{17} = \frac{1}{2}(\beta_2 - \beta_3 + \beta_5 - \beta_6)$
18	CH_3 antisymmetric deformation	$S_{18} = 12^{-1/2}(2\alpha_1 - \alpha_2 - \alpha_3 + 2\alpha_4 - \alpha_5 - \alpha_6)$
19	CH_3 antisymmetric deformation	$S_{19} = \frac{1}{2}(\alpha_2 - \alpha_3 + \alpha_5 - \alpha_6)$
20	CH_3 torsion	$S_{20} = 2^{-1/2}(\tau_2 + \tau_3)$
A''		
21	Si–C antisymmetric stretch	$S_{21} = 2^{-1/2}(R_2 - R_3)$
22	CH_3 antisymmetric stretch	$S_{22} = 2^{-1/2}(s_7 - s_8)$
23	CH_3 symmetric stretch	$S_{23} = 6^{-1/2}(d_1 + d_2 + d_3 - d_4 - d_5 - d_6)$
24	CH_3 antisymmetric stretch	$S_{24} = 12^{-1/2}(2d_1 - d_2 - d_3 - 2d_4 + d_5 + d_6)$
25	CH_3 antisymmetric stretch	$S_{25} = \frac{1}{2}(d_2 - d_3 - d_5 + d_6)$
26	C–Si–Cl deformation	$S_{26} = 2^{-1/2}(\Xi_2 - \Xi_3)$
27	C–Si–C deformation	$S_{27} = 6^{-1/2}(\Phi_2 - \Phi_3)$
28	CH_2 twist	$S_{28} = \frac{1}{2}(\gamma_1 - \gamma_2 - \theta_1 + \theta_2)$
29	CH_2 rock	$S_{29} = \frac{1}{2}(\gamma_1 - \gamma_2 + \theta_1 - \theta_2)$
30	CH_3 symmetric deformation	$S_{30} = 12^{-1/2}(\beta_1 + \beta_2 + \beta_3 - \alpha_1 - \alpha_2 - \alpha_3 - \beta_4 - \beta_5 - \beta_6 + \alpha_4 + \alpha_5 + \alpha_6)$
31	CH_3 antisymmetric deformation	$S_{31} = 12^{-1/2}(2\beta_1 - \beta_2 - \beta_3 - 2\beta_4 + \beta_5 + \beta_6)$
32	CH_3 antisymmetric deformation	$S_{32} = \frac{1}{2}(\beta_2 - \beta_3 - \beta_5 + \beta_6)$
33	CH_3 antisymmetric deformation	$S_{33} = 12^{-1/2}(2\alpha_1 - \alpha_2 - \alpha_3 - 2\alpha_4 + \alpha_5 + \alpha_6)$
34	CH_3 antisymmetric deformation	$S_{34} = \frac{1}{2}(\alpha_2 - \alpha_3 - \alpha_5 + \alpha_6)$
35	CH_2Cl torsion	$S_{35} = \tau_1$
36	CH_3 torsion	$S_{36} = 2^{-1/2}(\tau_2 - \tau_3)$

were observed in which the calculated *anti* and *gauche* fundamentals were separated more than 8 cm^{-1}. Frequently, the observed *anti/gauche* band pairs appeared at these particular frequencies. For the remaining 13 fundamentals below 1300 cm^{-1} the calculated *anti* and *gauche* were closely spaced and may overlap in the spectra.

The following eight observed band pairs (wavenumbers observed in Raman spectra of the liquid): 1183*/1176, 1107*/1098, 833*/825, 815/805*, 693*/685, 622/614*, 490*/481 and 297*/264 cm^{-1} (the bands with asterisks vanished in the infrared and/or Raman spectra of the crystal) were correlated with the scaled, calculated wavenumbers of the *anti* and *gauche* conformers (Tables 3 and 4). On a qualitative basis it was found that in seven instances the observed bands with asterisks made a better fit with those calculated for *gauche* and the remaining bands with *anti*, while for the band pair at 490*/481 cm^{-1} the opposite fit was preferable.

In a quantitative test we have selected the 8 bands with asterisks: 1183, 1107, 833, 805, 693, 614, 490 and 297 cm^{-1} and compared them with the scaled fundamentals ν_{16}, ν_{17}, ν_{19}, ν_{20}, ν_{23}, ν_{25}, ν_{27} and ν_{28} of the *gauche* rotamer (Table 4) and *anti* (Table 3). The sums of the differences between the observed and calculated bands were 98 cm^{-1} for *gauche* and 119 cm^{-1} for *anti*. This comparison suggests that the disappearing bands make a better fit with the calculated *gauche* than with the *anti* conformer. Therefore, *anti* should remain in the crystal and be the low energy rotamer in the liquid and in the matrices as also suggested qualitatively by the band pairs described above. It was reported by Sera *et al.*[8] that the infrared band at 692 cm^{-1} vanishing in the crystal, was enhanced in the polar solvent acetonitrile compared to the unpolar solvent carbon disulfide. Since the dipole moment of CDCS is determined by the C–Cl and Si–Cl bond moments, the *gauche* conformer should have a much higher dipole moment than *anti*. Therefore the *gauche* conformer should be stabilized in polar solvents,[8] in agreement with the assignments.

It should be emphasized that although the *ab initio* calculations reveal *anti* to be the low energy conformer

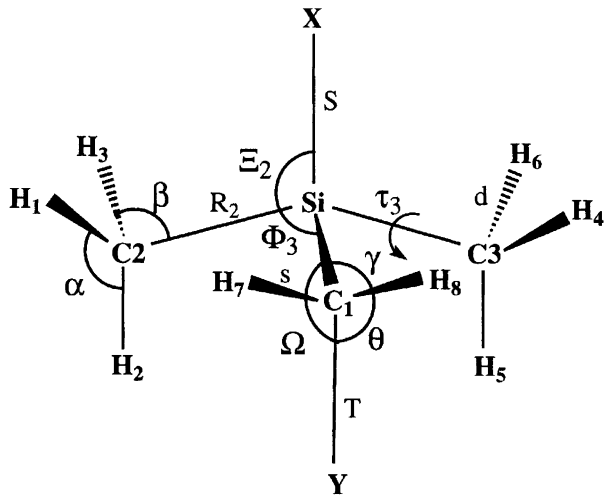

Fig. 13. Internal coordinates of CDCS.

in the whole series of halomethyl dimethyl halosilanes[22] [CH_2Y–$(CH_3)_2SiX$] it is by no means self-evident that *anti* is the low energy conformer of CDCS in the liquid. Thus, in both chloromethyl dimethyl fluorosilane[23] and bromomethyl dimethyl fluorosilane[24,25] gauche is the low energy conformer in the liquid and remains in the crystal. In the matrices, however, and probably also in the vapours, *anti* is the low energy conformer. In both of these molecules the polar *gauche* rotamer is stabilized compared to the unpolar *anti* in the liquid state relative to the vapour.

Spectral assignments. The assignments of the infrared and Raman spectra of CDCS to the *anti* and *gauche* conformers appear in Tables 1, 3 and 4. In order to make a comparison between the fundamentals of the *anti* and *gauche* conformers easier, they have been numbered consecutively for both conformers, rather than the conventional numbering in *anti* with those of species *A'* listed before *A''*.

The vibrational spectra of CDCS should have eight C–H stretching fundamentals ν_1–ν_8 belonging to each conformer, involving the hydrogen atoms of the methyl and methylene groups in CDCS. These modes are frequently accidentally degenerate and in addition all the fundamentals of *anti* overlap those of *gauche* in agreement with the scaled, calculated fundamentals. They were assigned to infrared and Raman bands between 2986 and 2908 cm^{-1}, while the weak or very weak bands below this region are interpreted as combination bands or overtones.

Similar to the C–H stretching region 3000–2900 cm^{-1}, the *ab initio* calculations reveal that the CH_3 deformation and the CH_2 scissoring and wagging modes should overlap considerably. The calculated, scaled wavenumbers suggest (Tables 3 and 4) that five fundamentals (ν_9–ν_{13}) for both conformers should be situated between 1440 and 1400 cm^{-1} while the four modes ν_{14}–ν_{17} were predicted between 1350 and 1100 cm^{-1}. We have assigned ν_9–ν_{15} for the *anti* and *gauche* conformers to the bands present both in the infrared and Raman spectra at 1437, 1413, 1400, 1260 and 1254 cm^{-1}, in which 1413 and 1400 cm^{-1} supposedly are accidentally degenerate. Except for the intense infrared bands around 1263 and 1255 cm^{-1} assigned to ν_{14} and ν_{15}, respectively, most of these bands were medium or weak both in the infrared and in the Raman spectra. Additional infrared bands around 1396, 1364 and 1267 cm^{-1} in the crystal with no Raman counterparts were supposedly combination bands.

The Raman bands at 1183 and 1176 cm^{-1} are assigned to the *gauche* and *anti* conformers of ν_{16} in accordance with the vanishing Raman band at 1180 cm^{-1} in the crystal, the reduced intensity of the infrared band in a Xe matrix at 1180 cm^{-1} and the van't Hoff plots based upon the Raman intensities at different temperatures. However, there is an infrared band at 1177 cm^{-1} in the crystal, possibly caused by a combination band of the *anti* conformer overlapping the fundamental. The band pairs at 1107 and 1098 cm^{-1} are without doubt attributed to the *gauche* and *anti* conformers, respectively, of ν_{17}. The infrared and Raman bands around 869 cm^{-1} were explained as combination bands rather than fundamentals.

The most intense infrared bands in the spectra of CDCS were observed in the region 860 to 810 cm^{-1}, caused by the close lying fundamentals ν_{18} and ν_{19}, in perfect agreement with the calculated infrared intensities of Tables 3 and 4. The *anti* and *gauche* modes ν_{18} were assigned to the bands at 854 and 846 cm^{-1} in the Xe matrix; they coincided in the spectra of the condensed phases. The band pair at 833 and 825 cm^{-1} in the Raman spectra were attributed to the *gauche* and *anti* conformers of ν_{19}. In the infrared spectra these conformers could hardly be distinguished at the intense peak at 828 cm^{-1}. The infrared and Raman bands around 814 and 805 cm^{-1} are attributed to the *anti* and *gauche* bands of ν_{20}.

The infrared and Raman bands around 758 and 705 cm^{-1} were both present in the crystals and each of them were assigned to overlapping *anti* and *gauche* conformer bands of ν_{20} and ν_{21}, respectively. In the Xe matrix spectra the intensity variations after annealing suggest a slight separation of the *anti* and *gauche* bands of these modes as apparent from Tables 1, 3 and 4. Bands around 693 and 685 cm^{-1} are undoubtedly the *gauche* and *anti* modes ν_{23}, whereas ν_{24} for both conformers coincide at 663 cm^{-1}. According to the calculations the *anti* and *gauche* conformers of ν_{24} should be separated by 19 cm^{-1}, and they are assigned to the bands at 622 and 614 cm^{-1}, which also makes a reliable band pair for the van't Hoff plots. Much more doubtful, ν_{26} of both conformers are assigned to the infrared bands around 575 cm^{-1} without any Raman counterpart.

The Raman bands at 490 and 481 cm^{-1} are attributed to the *anti* and *gauche* conformers of ν_{27}, while the intense infrared bands around 483 cm^{-1} of the amorphous and crystalline sample give no clue to the conformers.

The band pair at 297 and 264 cm^{-1} is assigned to ν_{28}, and gives the most reliable enthalpy values in the van't Hoff plots applied both to peak heights and band areas (Fig. 12). A number of skeletal bending modes ν_{29}–ν_{35} are attributed to the infrared and Raman bands between 250 and 120 cm^{-1}. All these bands consisted of coinciding *anti* and *gauche* contributions in the condensed phases, and no matrix spectra, which might reveal separate conformer bands, were recorded in this frequency range.

The two methyl torsions ν_{33} and ν_{34}, which are accidentally near degenerate and coinciding for the two conformers, are assigned to the weak Raman band around 168 cm^{-1} in the liquid. The CH_2Cl torsional modes for the *anti* and *gauche* conformers, ν_{36}, are expected in the range 60–70 cm^{-1} from the calculations, and they are tentatively both attributed to the Raman band detected at 80 cm^{-1} in the liquid, well established in the $R(\nu)$ representation (Fig. 11).

Acknowledgment. We are grateful to Mrs. Anne Horn for very valuable assistance.

References

1. Krieble, R. H. and Elliot, J. R. *J. Am. Chem. Soc. 67* (1945) 1810.
2. McBride, J. J. and Beachell, H. C. *J. Am. Chem. Soc. 70* (1948) 2532.
3. Speier, J. *J. Am. Chem. Soc. 73* (1951) 824.
4. Hayashi, M. *Nippon Kagaku Zassahi 79* (1956) 508.
5. Batvev, M. I., Ponomarenko, V. A., Matveeva, A. D. and Snegova, A. D. *Izvest Akad. Nauk SSSR, Otdel. Khim. Nauk* (1958) 996.
6. Goubeau, J., Hein, G. R. and Hein, I. *Z Anorg. Allg. Chem. 312* (1961) 110.
7. Kriegsmann, H. and Engelhardt, G. E. *Z. Chem. 2* (1962) 95.
8. Sera, K., Suehiro, K., Hayashi, M. and Murata, M. *Bull. Chem. Soc. Jpn. 49* (1976) 29.
9. Ernst, M., Schenzel, K., Jähn, A. and Hassler, K. *J. Mol. Struct. In press.*
10. Ernst, M., Schenzel, K., Jähn, A., Köll, W. and Hassler, K. *J. Raman Spectrosc. 28* (1997) 589.
11. Sullivan, J. F., Qtaitat, M. A. and Durig, J. R. *J. Mol. Struct. (Theochem) 202* (1989) 159.
12. Durig, J. R., Sullivan, J. F. and Qtaitat, M. A. *J. Mol. Struct. 243* (1991) 239.
13. Qtaitat, M. A. and Durig, J. R. *Spectrochim. Acta, Part A 49* (1993) 2139.
14. Afifi, M. S., Guirgis, G. A., Mohamed, T. A., Herrebout, W. A. and Durig, J. R. *J. Raman Spectrosc. 25* (1994) 159.
15. Durig, J. R., Guirgis, G. A., Mohamed, T. A., Herrebout, W. A. and Afifi, M. S. *J. Mol. Struct. 319* (1994) 109.
16. Jensen, H. M., Klaeboe, P., Guirgis, G. A., Aleksa, V., Nielsen, C. J. and Durig, J. R. *J. Mol. Struct. 410–411* (1997) 483.
17 Miller, F. A. and Harney, B. M. *Appl. Spectrosc. 24* (1970) 291.
18. Guirgis, G. A., Nilsen, A., Klaeboe, P., Aleksa, V., Nielsen, C. J. and Durig, J. R. *J. Mol. Struct. 410–411* (1997) 477.
19. Barnes, A. J. *J. Mol. Struct. 113* (1984) 161.
20. Nielsen, O. Faurskov, *Annu. Rep. Progr. Chem., Sect. C 90* (1993) 3.
21. Gaussian 94, Revision D.2: Frisch, M. J., Trucks, G. W., Schlegel, H. B., Gill, P. M. W., Johnson, B. G., Robb, M. A., Cheeseman, J. R., Keith, T., Petersson, G. A., Montgomery, J. A., Raghavachari, K., Al-Laham, M. A., Zakrzewski, V. G., Ortiz, J. V., Foresman, J. B., Cioslowski, J., Stefanov, B. B., Nanayakkara, A., Challacombe, M., Peng, C. Y., Ayala, P. Y., Chen, W., Wong, M. W., Andre, J. L., Replogle, E. S., Martin, R., L., Fox, D. J., Binkley, J. S., Defrees, D. J., Baker, J., Stewart, J. P., Head-Gordon, M., Gonzalez, C. and Pople, J. A., Gaussian, Inc., Pittsburgh, PA 1995.
22. Klaeboe, P. *J. Mol. Struct. 408–409* (1997) 81.
23. Aleksa, V., Klaeboe, P., Nielsen, C. J. and Guirgis, G. A. *J. Mol. Struct. In press.*
24. Jensen, H. M., Klaeboe, P., Nielsen, C. J., Aleksa, V., Guirgis, G. A. and Durig, J. R. *J. Mol. Struct. 410–411* (1997) 489.
25. Jensen, H. M., Guirgis, G. A., Klaeboe, P., Nielsen, C. J. and Aleksa, V. *Acta Chem. Scand. Submitted.*

Received June 23, 1997.